On the variation of the maximum crystal nucleation rate temperature with glass transition temperature

Article *in* Journal of Non-Crystalline Solids · June 2016

DOI: 10.1016/j.jnoncrysol.2016.03.024

3 authors, including:

Daniel Cassar
Universidade Federal de São Carlos
5 PUBLICATIONS **4** CITATIONS

SEE PROFILE

Edgar Dutra Zanotto
Universidade Federal de São Carlos
294 PUBLICATIONS **4,732** CITATIONS

SEE PROFILE

On the variation of the maximum crystal nucleation rate temperature with glass transition temperature

Prabhat K. Gupta*, Daniel R. Cassar, and Edgar D. Zanotto
Vitreous Materials Laboratory (LaMaV)
Department of Materials Engineering
Federal University of São Carlos, São Carlos, SP, Brazil

(*) Professor Emeritus
The Ohio State University
Columbus, OH, USA 43210

Abstract:

The variation of the maximum nucleation rate temperature (T*) with respect to the glass transition temperature (T_g) is analyzed as a function of system parameters such as fragility. Calculated values are compared with experimental results for six stoichiometric oxide systems that are known to exhibit homogeneous nucleation. An examination of T*(T_g) relation supports the experimental observation that liquids having T* > T_g tend to exhibit homogeneous nucleation whereas only heterogeneous nucleation is observed in other systems.

1. INTRODUCTION

Below the melting temperature (T_M), a liquid is metastable against the stable crystal state. The crystal nucleation rate in a super-cooled liquid shows a maximum at some temperature (T*) before vanishing at low temperatures[1]. There is considerable interest in understanding how T* varies with various system parameters[2,3]. The maximum nucleation rate temperature plays an important role in the design of nano-structured glass-ceramics[4]. More importantly, as observed by James[5] and by Zanotto[6], it is a signature of the nucleation ability of a liquid. Systems having T* greater than the glass transition temperature (T_g) tend to exhibit (in commonly accessible laboratory time/sample-size scales) homogeneous (internal or volume) nucleation while others, having $T^* < T_g$, show only heterogeneous (surface) nucleation. This suggests that the glass forming ability is better for systems having $T^* < T_g$. This paper reports an analysis of the variation of T* with T_g as a function of system parameters such as fragility. The calculations are compared with experimental data in six stoichiometric oxide glass formers. These are the only (to our knowledge) stoichiometric oxide systems where homogeneous nucleation has been documented and for which sufficient thermodynamic and kinetic data are available to make the necessary calculations.

Similar to previous reported efforts in the literature[5–8] the present analysis uses a formalism based on the classical nucleation

theory (CNT) in combination with the Stokes-Einstein (SE) equation for the atomic transport involved in nucleation, the Vogel–Fulcher–Tammann (VFT) expression for the temperature dependence of viscosity, and the Turnbull expression for the thermodynamic driving force for crystal nucleation. As has been pointed out[9], there are some fundamental issues with this phenomenology. While the failures of CNT in predicting absolute values of nucleation rates are well known[10,11], several investigations[5,7,12] have reported that the temperature dependence of the nucleation rate is well described by CNT, at least in the temperature range above T*. Similarly, the SE and Turnbull equations are questionable approximations[13] but have been used frequently[2,7,8] to provide qualitative (i.e., generic) description of nucleation kinetics. The validity of VFT is also controversial (especially at very low temperatures, $T < T_g$) despite the fact that it fits the viscosity data well above T_g[14,15]. In spite of these shortcomings, several investigators[5,7] have successfully used this formalism to examine the temperature dependence of the nucleation kinetics in stoichiometric oxide melts. Our motivation to use of this formalism lies in the fact that it permits quantitative results about the variation of T* with T_g with a mathematical rigor (i.e., with no subsequent mathematical simplifications or approximations) that has not been reported in previous works. In principle, the present treatment can be extended to more complex formalisms (non-SE, non-VFT and non-Turnbull) but not without a significant loss of clarity and rigor.

2. LITERATURE REVIEW

As early as 1986, Weinberg[16] analyzed the dependence of T* on system parameters using CNT. Weinberg showed that in general $T^* \geq T_M/3$ (where T_M is the melting temperature of the crystal phase). This analysis showed that two dimensionless parameters (a reduced activation energy of viscous flow and the ratio of the difference in specific heat between the liquid and the crystal to the entropy of fusion) control the location of T*. In addition, he showed that T* is dominated by (and increases with increase in) the activation energy of viscous flow. However, Weinberg's analysis used an Arrhenius temperature dependence of the viscosity that is limited to "strong" liquids and employed an approximate form of the Stokes–Einstein equation to account for the atomic re-arrangements controlling crystal nucleation in the liquid. The effects of these approximations are not clear on his results.

Later, Zanotto and Weinberg (ZW)[8] used the Stokes–Einstein equation in combination with the non-Arrhenius VFT temperature dependence of viscosity to calculate (numerically) the values of T* for selected stoichiometric oxide glass compositions. Based on these results, ZW made the important observation: only glasses having $T^* > T_g$ exhibited internal (homogeneous) nucleation in laboratory time/size scales. However, ZW did not perform an analytic variation of T* as a function of system parameters. Fokin et al.[2] reported experimental evidence that, in silicate melts that undergo internal nucleation, T* is typically close to (equal or greater than) T_g.

Unfortunately, they also used an approximate form of the Stokes–Einstein equation to rationalize the dependence of T* on T_g. Recently, Schmelzer et al.[3] have analyzed the variation of T* (as well as the temperatures of maximum growth rate and that of overall crystallization rate). While their calculated results for T* are similar to the results reported in this paper, they did not use the Stokes–Einstein or the VFT equations. Further, they introduced an unconventional definition of fragility that makes their results difficult to compare with the conventional fragility data. To our knowledge, a rigorous analysis of T* as a function of T_g and fragility is not available in the literature.

3. ANALYSIS

i) ***The VFT expression for the T-dependence of viscosity, $\eta(T)$*:**

The VFT expression[17–19] is an empirical non-Arrhenius equation that exhibits viscosity divergence at a finite temperature T_0 - called the VFT temperature. Using a reduced temperature, x, that is normalized with respect to the melting temperature, T_M of the crystal phase:

$$x \equiv \frac{T}{T_M} \quad , \tag{1}$$

the VFT equation can be expressed as follows:

$$\ln(\eta) = A + \frac{C_2}{x - x_0} \quad , \tag{2}$$

where A, C_2 (the dimensionless activation energy), and $x_o = T_0/T_M$ (the reduced VFT temperature) are the three VFT parameters. The VFT equation can also be expressed in terms of experimentally accessible system parameters, such as the reduced glass transition temperature and fragility. Using eqn 2, the reduced glass transition temperature, x_g (defined as the temperature where the value of viscosity, η_g, is 10^{12} Pa.s) is given by:

$$x_g = x_0 + \frac{C_2}{D} \quad . \qquad (3)$$

Here, the constant $D \equiv \left[\ln(\eta_g) - A\right]$ has a fixed value of approximately 37. Using eqn 3, the VFT eqn can be expressed in terms of x_g:

$$\ln(\eta) = A + D\frac{x_g - x_0}{x - x_0} \quad . \qquad (4)$$

It is also possible to write the VFT eqn in terms of the fragility (m) of the system, which is defined[20] as:

$$m = \left.\frac{\partial \log_{10}(\eta)}{\partial\left(\frac{x_g}{x}\right)}\right|_{x=x_g} \quad . \qquad (5)$$

Using eqn 4, it can be readily shown that

$$x_0 = x_g\left[1 - \frac{m_0}{m}\right] \quad , \qquad (6)$$

where m_o, the minimum value of fragility (corresponding to the strongest liquid), is about 16 and is related to D as follows:

$$D = m_0(\ln(10)) \quad . \tag{7}$$

Eliminating x_o between eqns 4 and 6 gives the VFT eqn that has m_o, x_g, and m as the three VFT parameters:

$$\ln(\eta) = A + \frac{m_0^2 \ln(10)}{m\left(\frac{x}{x_g} - 1\right) + m_0} \quad , \tag{8}$$

where A and m_o are related as follows:

$$A = (12 - m_0)(\ln(10)) \quad . \tag{9}$$

ii) ***Expression for the T-dependent steady state nucleation rate****:*

When combined with the Stokes-Einstein equation, CNT gives the following expression for the steady state nucleation rate, I(T):

$$I(T) = \frac{KT}{\eta(T)} \exp\left[-\left(\frac{W(T)}{k_B T}\right)\right] \tag{10}$$

Here *K* is a constant and k_B is the Boltzmann constant. For a spherical nucleus, the thermodynamic barrier, W, is given by:

$$W(T) = \frac{16\pi\sigma^3}{3\Delta G_V^2(T)} \quad . \tag{11}$$

Here σ is the surface energy density of the crystal-liquid interface. According to the Turnbull expression[21], which gives an upper bound for the free energy change per unit volume, ΔG_V, is expressed in terms of the enthalpy of melting, ΔH_M:

$$\Delta G_V = \frac{\Delta H_M}{V}\left[1 - \frac{T}{T_M}\right] \quad . \tag{12}$$

Here V is the molar volume. Combining eqns 1, 11, and 12, one can rewrite W as follows:

$$\frac{W}{k_B T} = \frac{C_1}{x(1-x)^2} \quad , \tag{13}$$

where the dimensionless positive parameter C_1, representing the thermodynamic barrier for nucleation, is given by

$$C_1 = \left(\frac{16\pi}{3}\right)\frac{\sigma^3 V^2}{k_B T_M (\Delta H_M)^2} \quad . \tag{14}$$

The value of the surface energy, σ, can be calculated via the Skapski-Turnbull equation[21–23]:

$$\sigma = \frac{\alpha \Delta H_M}{\sqrt[3]{N_A V_M^2}} \quad . \tag{15}$$

Where α is a non-dimensional parameter, ($0.4 < \alpha < 0.5$), for homogeneous nucleation in supercooled liquids and N_A is Avogadro´s number and V_M is the molar volume of the crystal phase.

Using eqns (2) and (13), eqn (10) for the nucleation rate becomes:

$$y(x) = \ln(x) - \frac{C_1}{x(1-x)^2} - \frac{C_2}{x - x_0} \quad , \tag{16}$$

where

$$y(x) \equiv A + \ln\left[\frac{I(x)}{K T_M}\right] \qquad (17)$$

iii) *Analysis for T* (T_g, system parameters):*

Our goal is to find, using eqn 16, the variation of x* (the value of x where y is maximized) as a function of the reduced glass transition temperature, x_g keeping C_1 (the reduced thermodynamic barrier) fixed. The variation of x* with x_g depends on which of the three kinetic parameters is held fixed: C_2, or x_o, or m.

a) Solution, $x^*(x_g, C_2)$, when C_2 is fixed:

Setting the derivative of eqn 16 with respect to x equal to zero and using eqn 3, gives the following result:

$$x_g = \frac{C_2}{D} + x^{\zeta} \pm \left[\frac{C_2 (x^{\zeta})^2 (1 - x^{\zeta})^3}{C_1 (3x^{\zeta} - 1) - x^{\zeta}(1 - x^{\zeta})^3}\right]^{1/2} \quad . \qquad (18)$$

We use the negative sign since it gives the correct expression for the special case when $x_o = 0$ (i.e., for strong liquids that exhibit Arrhenian viscosity). Thus, for the case of constant C_2, one gets an explicit solution for $x_g(x^*, C_2)$:

$$x_g = \frac{C_2}{D} + x^{\zeta} - \left[\frac{C_2 (x^{\zeta})^2 (1 - x^{\zeta})^3}{C_1 (3x^{\zeta} - 1) - x^{\zeta}(1 - x^{\zeta})^3}\right]^{1/2} \quad . \qquad (19)$$

This equation can be numerically inverted to give $x^*(x_g, C_2)$.

b) Solution, $x^*(x_g, x_o)$, when x_o is fixed:

By combining eqn 3 with eqn 19, we obtain the following expression for $x_g(x^*, x_o)$:

$$x_g = x_0 + \left\{ \frac{(x_0 - x^*)^2 \left[C_1 (3x^* - 1) - x^* (1 - x^*)^3 \right]}{D (x^*)^2 (1 - x^*)^3} \right\} \quad . \qquad (20)$$

As with eqn 19, eqn 20 can be numerically inverted to yield $x^*(x_g, x_o)$.

c) Solution, $x^*(x_g, m)$, when fragility (m) is fixed:

For the case of constant fragility (m), combining eqn 6 with eqn 20 gives the following result for $x_g(x^*, m)$:

$$x_g = \frac{-b + \sqrt{b^2 - 4\left[1 - \left(\frac{m_0}{m}\right)\right]^2 (x^*)^2}}{2\left[\left(1 - \frac{m_0}{m}\right)\right]^2} \qquad (21)$$

where

$$b = -2x^* \left(1 - \frac{m_0}{m}\right) - \frac{m_0^2}{m} \ln(10) \left[\frac{(x^*)^2 (1 - x^*)^3}{C_1 (3x^* - 1) - x^* (1 - x^*)^3} \right] \quad . \qquad (22)$$

Eqns 21 and 22 can be solved for x_g as a function of x* for a given value of m (> m_o). The result can then be inverted to plot x* as a function of x_g for a value of m greater than m_o.

For the special case of strong liquid (i.e., for m = m_o), the solution given by eqn 21 reduces to eqn 20 with x_o = 0:

$$x_g(m=m_0)=\frac{C_1(3x^*-1)-x^*(1-x^*)^3}{D(1-x^*)^3} \quad . \qquad (23)$$

In addition, for the special case of extremely fragile liquid when m approaches infinity, eqn 21 reduces to (for x_g > 1/3):

$$x_g(m\to\infty)=x^* \quad . \qquad (24)$$

4. **RESULTS**

The calculations are performed for x* as a function of x_g using a value of D = 37. The results are shown in figures 1 – 3.

Figure 1 shows values of x*, at fixed values of C_1 and C_2 calculated using equation 19, plotted as a function of x_g for four combinations of (C_1, C_2) values: (6,2), (6,4), (10,2), and (10,4). As shown in Table I, these ranges of C_1 and C_2 values cover the range typical of silicate glass-formers. According to equation 3, a variation of x_g when holding C_2 fixed is equivalent to a variation in x_o. Thus Figure 1 is effectively a plot of x* versus x_o for fixed C_1 and C_2.

Table I: Values of calculated parameters. Uncertainties obtained from nonlinear regression of the viscosity data (one standard deviation) are given by the number in the parentheses and represent the

precision in the last digit. Uncertainties in C_2 and m/m_0 were obtained via linear error propagation.

Composition	C_1	C_2	x*	x_0	x_g	x_g (Eq 20)	m/m_0
$Li_2Si_2O_5$	8.6	5.8(2)	0.56	0.382(4)	0.555(7)	0.57	3.2(1)
$BaSi_2O_5$	4.1	5.54(8)	0.58	0.412(2)	0.569(3)	0.51	3.63(7)
$CaSiO_3$	5.8	3.9(1)	0.58	0.461(3)	0.571(5)	0.52	5.2(2)
$Na_2Ca_2Si_3O_9$	11	7.6(3)	0.55	0.340(7)	0.53(1)	0.62	2.8(1)
$Na_4CaSi_3O_9$	8.4	4.7(2)	0.55	0.395(6)	0.532(9)	0.52	3.9(2)
$Ba_2TiSi_2O_8$	11	3.80(8)	0.59	0.472(2)	0.575(3)	0.61	5.6(2)

Figure 2 shows x^* calculated using eqn 20 as a function of x_g for fixed values of C_1 and x_o. The variation of x_g, at fixed x_o, is because of variation in C_2. Two different values of x_o (0.3 and 0.4) and two values of C_1 (6,10), which cover the range of typical values reported for a number of silicate glasses, are used in this figure.

Figure 3 shows calculated x* plotted as a function of x_g for fixed values of C_1 and fragility (m). Two different values of C_1 (6 and 10) and three different values of the ratio m/m_o (= 1, 3, and 6) are used. It should be emphasized that the dashed line $x^* = x_g$ (for $x_g > 1/3$) corresponds to the case of an infinitely fragile liquid (i.e., $m \rightarrow \infty$). The intercept of x* at $x_g = 0$, although appears to be the same for all curves in figure 3, actually decreases somewhat with increase in C_1 but is independent of the value of m. For example, for $C_1 = 6$ the intercept x* value is 0.3388 and for $C_1 = 10$, the intercept value is 0.3366.

Also shown in these figures are the experimental data points for six stoichiometric silicate melts where homogenous nucleation has been observed experimentally. The values of various parameters for these six systems are listed in Tables I and II using published data from various sources (see Table II for the references).

Table II: Experimental data on six stoichiometric compositions. Viscosity data was used to obtain the VFT parameters A, B (= C_2T_M), and T_0 and T_g (temperature were the viscosity is equal to 10^{12} Pa.s). σ calculated via Eq. (15) considering α = 0.45(5). References are given by the numbers in the brackets. Numbers inside parentheses represent the precision in the last digit.

Composition	$Li_2Si_2O_5$	$BaSi_2O_5$	$CaSiO_3$	$Na_2Ca_2Si_3O_9$	$Na_4CaSi_3O_9$	$Ba_2TiSi_2O_8$
$V_m \times 10^{-05}$ (m^3/mol)	6.39** [24]	7.39 [38]	3.99** [42]	12.9* [51]	13.5* [54]	11.4 [59]
T^* (K)	732 [7,25–31]	984 [7,39,40]	1050 [43]	856 [12,52]	778 [55]	1014 [60,61]
T_g (K)	725(9)	963(5)	1039(9)	834(18)	755(13)	985(5)
T_M (K)	1306 [32]	1693 [37]	1821 [44]	1564 [12]	1418 [56]	1715 [62]
T_0 (K)	499(6)	698(4)	840(6)	532(11)	560(8)	809(3)
B (K)	7600(200)	9400(100)	7200(200)	11900(500)	6700(300)	6500(100)
A (ln of Pa.S)	-5.8(2)	-7.7(1)	-8.4(2)	-11.8(4)	-6.8(3)	-9.3(1)
σ (J/m2)	0.20(2)	0.11(1)	0.26(3)	0.19(2)	0.13(1)	0.24(3)
ΔH_m (J/mol)	61086 [33]	37500 [7]	57300 [45]	91211 [53]	64860 [57]	106000 [63]
Viscosity Refs.	[7,25,29, 34–37]	[7,37,39,41]	[46–50]	[12,52]	[55,58]	[64–66]

* Molar volume from glass.
** Estimated from XRD data

5. DISCUSSION

To begin with, we emphasize that equations 19, 20, and 21 apply only for nucleation in the equilibrium supercooled liquid state and not in the non-equilibrium glassy state. The thermodynamic and transport properties of the glassy state are much different than those of the super-cooled liquid state and the effects of freezing of liquid into a glass (i.e., glass transition) on the nucleation rate are not considered here. However, the supercooled liquid state can be achieved for $T < T_g$, as long as the observation times are greater than the required

time for the structure to relax. Indeed, the nucleation experiment times are typically much longer than such structural relaxation times.

For the formalism used, the value of x* depends on a thermodynamic parameter C_1 and two kinetic parameters. One kinetic parameter is x_g and the second can be either C_2 or x_o or the fragility, m. Depending on the choice of the second kinetic parameter, one obtains different results for $x^*(x_g)$. The results for each of the three choices are shown in Figures 1 – 3 (where C_1 is held fixed). Even though these figures appear different, they have equivalent information. The difference is because Figure 1 is a plot at constant C_2 (i.e., a constant value of the difference $(x_g - x_o)$). On the other hand, figure 2 is for constant values of x_o, and figure 3 is at constant value of fragility (i.e., at constant value of the ratio x_o/x_g). Several common features of these figures are worth noting:

1) The maximum nucleation rate temperature, x*, always increases with increase in x_g. This is consistent with experimental observations as shown by the six experimental data points. Table I shows that experimental values of x* are higher for systems having higher values of x_g (compositions $BaSi_2O_5$ and $Ba_2TiSi_2O_8$). The x* value is smallest for the $Na_4CaSi_3O_9$ composition for which x_g is smallest. Fokin et al.[2] have made similar observation.

2) The temperature, x*, is greater than x_g only for small values of x_g. At higher values of x_g, x* becomes less than x_g. The value of the cross-over temperature (which we label $\underline{x}_g$) is the same, for a given

system, in all three figures. It is possible to solve for $\underline{x}_g$. For example, for the case of fixed x_o, it can be shown, using eqn 20, that the cross-over $\underline{x}_g$ satisfies the following eqn:

$$C_1 = \frac{1}{3\underline{x}_g - 1}\left[\underline{x}_g\left(1-\underline{x}_g\right)^3 + \frac{D\,\underline{x}_g^2\left(1-\underline{x}_g\right)^3}{\left(\underline{x}_g - x_0\right)}\right] \quad . \qquad (25)$$

As an example, we show in Figure 4, calculated values of $\underline{x}_g$ as a function of C_1 for two different values of x_o using eqn 25. For example, for x_o = 0.4 and C_1 = 10, $\underline{x}_g$ is about 0.55. The value of $\underline{x}_g$ increases with increase in x_o and with decrease in C_1. For a fixed value of x_o, smaller values of C_1 (thermodynamic barrier) increase the value of $\underline{x}_g$ and thus the range over which x* is greater than x_g. Similar analysis can be carried out for the case of fixed fragility. As shown in figure 3, the cross-over $\underline{x}_g$ increases significantly with increase in fragility at a constant value of C_1.

3) The data points in figures 1, 2, and 3 correspond to experimentally observed values of x* and x_g for six stoichiometric oxide systems that are known to nucleate homogeneously in laboratory / size scales. As shown in table I, the observed x* values for these systems range from 0.55 to 0.59 while the x_g values range from 0.53 to 0.57. The six points are close to (but slightly above) the x* = x_g line. Zanotto[6] has shown that systems that show heterogeneous nucleation tend to have x* < x_g and, for these systems, x_g values are higher, typically in the range 0.6 to 0.7.

It is important to point out that these experimental data points are not in full agreement with the results of our calculations. In table I, we show values of x_g calculated using eqn 20 and experimental values of x^* and x_o. The agreement is excellent for the Lithium disilicate system. For three other systems ($CaSiO_3$, $Na_4CaSi_3O_9$, and $Ba_2TiSi_2O_8$) the agreement between observed x_g and calculated x_g values is within 10%. For the remaining two compositions ($BaSi_2O_5$ and $Na_2Ca_2Si_3O_9$), the agreement is poor. The reason for this disagreement is most likely because of the fairly substantial uncertainties in the thermodynamic and interfacial tension data shown in table II but could also be due to the shortcomings of the phenomenology used (i.e., the combination of CNT/SE/VFT/Turnbull expression).

4) As mentioned earlier, James[5], and Zanotto and Weinberg[8] have noted that systems having x^* greater than x_g tend to exhibit homogeneous nucleation (in addition to heterogeneous nucleation) while others (having x^* less than x_g) show only heterogeneous nucleation. This observation is supported by the present results.

Since heterogeneous nucleation effectively occurs at reduced values of interfacial energy (i.e., lower values of C_1), the heterogeneous nucleation rate is frequently, but not always, larger than the homogeneous nucleation rate. This is because the number of available nucleation sites is always much smaller for heterogeneous than homogeneous nucleation. In general, even if homogeneous nucleation is not observed in the bulk of a sample, heterogeneous nucleation has most likely occurred on the surface (or other

heterogeneous sites) of the sample. Heterogeneous nucleation can easily be detected because the nucleation rate versus temperature curve (and its maximum) is always shifted to higher temperatures when compared to homogeneous nucleation in the same liquid. Further, above T_g the nucleation time lag (time period necessary for the system to reach a steady-state distribution of embryos) for heterogeneous nucleation are short enough, i.e. below the typical laboratory time scales[2].

Observation of homogeneous nucleation is simply a matter of having the overall non-steady state homogeneous nucleation rate (after accounting the time lag) that is larger than some critical rate below which homogeneous nucleation will not be observed in the laboratory time/size scales. A conservative estimate of this critical rate is about 10^3 m^{-3} s^{-1}. In addition, the nucleation time-lags must be short enough, e.g. below a few days.

According to our analysis, there are three factors that support the notion that homogeneous nucleation is less likely to be observed when x* is less than x_g. These are:

a) The magnitude of the maximum nucleation rate decreases as x* increases. This can be seen by substituting x* for x in eqn 16. Note that the first term on the right hand side (the ln(x) term) is not significant. This result is also clear in the calculations of Fokin et al[2] (see their figure 3) of homogeneous nucleation rates. Thus it

becomes more difficult to observe homogeneous nucleation when x* is large.

b) Only at higher values, x* becomes less than x_g (for values of x_g greater than the crossover value $\underline{x}_g$).

c) Eqn 16 shows that the magnitude of the maximum nucleation rate decreases as C_1 increases. In addition, as shown in figure 4, a high value of C_1 gives rise to a lower value of the cross-over $\underline{x}_g$ and, therefore, to a larger range of x_g values over which x* is less than x_g.

Another important factor, which was not explored in this short article, but was demonstrated earlier by Fokin et al.[2], is that the nucleation time-lags are very long for compositions having $x^* < x_g$. These long time lags also preclude the experimental observation of homogenous nucleation in the high T_g (high x_g) glasses. The net result of these factors is that when $x^* < x_g$, the chances of observing homogeneous nucleation in laboratory time/size scales dramatically diminish. This result is indeed confirmed by experiments.

CONCLUSIONS

Despite its shortcomings in predicting the magnitudes of the steady-state nucleation rates, CNT may be useful for the analysis of qualitative trends among features of the nucleation process that do not involve absolute homogeneous nucleation rate values. For

example, the equations derived here and associated calculations show that, when combined with experimental viscosity data and calculated values of the thermodynamic driving force and surface energy, CNT predicts that the temperature of maximum nucleation rate x* increases (and the magnitudes decrease) with increasing x_g. In addition, we show that x* increases with increase in fragility (for a given value of the normalized thermodynamic barrier) and decreases with increase in the thermodynamic barrier (for a given value of fragility). These trends also agree with experimental observations.

Further, our calculations support the observation that for $x^* < x_g$, homogeneous nucleation is less likely to be observed.

Acknowledgements:

Prabhat K. Gupta gratefully acknowledges the São Paulo State Research Foundation, FAPESP support (# 2015/01848-9) for his visit to LaMaV, UFSCar, São Carlos, Brazil from July 1 through September 30, 2015. Daniel R. Cassar gratefully acknowledges the Brazilian National Research Council, CNPq (# 150490/2015-1). Edgar D. Zanotto is grateful to the São Paulo State Research Foundation, FAPESP (# 2013/07793-6) for funding this research work.

REFERENCES:

[1] See for example, K. Kelton and A.L. Greer, Nucleation in Condensed Matter: Applications in Materials and Biology (Elsevier, 2010) p. 42.

[2] V.M. Fokin, E.D. Zanotto, and J.W.P. Schmelzer, J. Non-Cryst. Solids **321**, 52 (2003).
[3] J.W.P. Schmelzer, A.S. Abyzov, V.M. Fokin, C. Schick, and E.D. Zanotto, J. Non-Cryst. Solids **429**, 24 (2015).
[4] E.D. Zanotto, Am. Ceram. Soc. Bull. **89**, 19 (2010).
[5] P.F. James, J. Non-Cryst. Solids **73**, 517 (1985).
[6] E.D. Zanotto, J. Non-Cryst. Solids **89**, 361 (1987).
[7] E.D. Zanotto and P.F. James, J. Non-Cryst. Solids **74**, 373 (1985).
[8] E.D. Zanotto and M.C. Weinberg, Phys. Chem. Glass. - Eur. J. Glass Sci. Technol. Part B **30**, 186 (1989).
[9] V.M. Fokin, E.D. Zanotto, N.S. Yuritsyn, and J.W.P. Schmelzer, J. Non-Cryst. Solids **352**, 2681 (2006).
[10] G.F. Neilson and M.C. Weinberg, J. Non-Cryst. Solids **34**, 137 (1979).
[11] E.G. Rowlands and P.F. James, Phys. Chem. Glas. **20**, 1 (1979).
[12] C.J.R. Gonzalez-Oliver and P.F. James, J. Non-Cryst. Solids **38–39, Part 2**, 699 (1980).
[13] J.W.P. Schmelzer, J. Non-Cryst. Solids **356**, 2901 (2010).
[14] J.C. Mauro, Y. Yue, A.J. Ellison, P.K. Gupta, and D.C. Allan, Proc. Natl. Acad. Sci. U. S. A. **106**, 19780 (2009).
[15] S.A. Kivelson and G. Tarjus, Nat. Mater. **7**, 831 (2008).
[16] M.C. Weinberg, J. Non-Cryst. Solids **83**, 98 (1986).
[17] H. Vogel, Phys. Z. **22**, 645 (1921).
[18] G.S. Fulcher, J. Am. Ceram. Soc. **8**, 339 (1925).
[19] G. Tammann and W. Hesse, Z. Für Anorg. Allg. Chem. **156**, 245 (1926).
[20] L.-M. Wang, C.A. Angell, and R. Richert, J. Chem. Phys. **125**, 4505 (2006).
[21] D. Turnbull, J. Appl. Phys. **21**, 1022 (1950).
[22] A.S. Skapski, J. Chem. Phys. **16**, 389 (1948).
[23] A.S. Skapski, Acta Metall. **4**, 576 (1956).
[24] F. Liebau, Acta Crystallogr. **14**, 389 (1961).
[25] Z. Zhenhua, J. Chin. Ceram. Soc. **2**, 003 (1987).
[26] J. Deubener, R. Brückner, and M. Sternitzke, J. Non-Cryst. Solids **163**, 1 (1993).
[27] P.F. James, Phys. Chem. Glass. **15**, 95 (1974).
[28] V.M. Fokin, A.M. Kalinina, and V.N. Filipovich, J. Cryst. Growth **52, Part 1**, 115 (1981).
[29] G.A. Sycheva, Glass Phys. Chem. **37**, 135 (2011).
[30] V.N. Filipovich and A.M. Kalinina, Neorganicheskie Mater. **7**, 1844

(1971).
[31] G.A. Sycheva, Glass Phys. Chem. **24**, 342 (1998).
[32] F.C. Kracek, J. Phys. Chem. **34**, 2641 (1929).
[33] K. Takahashi and T. Yoshio, J. Ceram. Assoc. Jpn. **81**, 524 (1973).
[34] M.R. Heslin and J.E. Shelby, Ceram Trans **30**, 189 (1992).
[35] R. Ota, T. Wakasugi, W. Kawamura, B. Tuchiya, and J. Fukunaga, J. Non-Cryst. Solids **188**, 136 (1995).
[36] C.J.R. Gonzalez-Oliver, P.S. Johnson, and P.F. James, J. Mater. Sci. **14**, 1159 (1979).
[37] J.O. Bockris, J.D. Mackenzie, and J.A. Kitchener, Trans. Faraday Soc. **51**, 1734 (1955).
[38] D.R. Lide and Chemical Rubber Company, editors , *CRC Handbook of Chemistry and Physics: A Ready-Reference Book of Chemical and Physical Data*, 90. ed., 2009 - 2010 (CRC Press, Boca Raton, FLa., 2009).
[39] A.M. Rodrigues, Diffusional processes in barium disilicate glass: crystallization, viscous flow, and relaxation, Ph.D. thesis, Universidade Federal de São Carlos, 2014.
[40] A.H. Ramsden and P.F. James, J. Mater. Sci. **19**, 1406 (1984).
[41] M. Lenoir, A. Grandjean, Y. Linard, B. Cochain, and D.R. Neuville, Chem. Geol. **256**, 316 (2008).
[42] T. Ito, R. Sadanaga, Y. Takéuchi, and M. Tokonami, Proc. Jpn. Acad. **45**, 913 (1969).
[43] L. Gránásy, T. Wang, and P.F. James, J. Chem. Phys. **108**, 7317 (1998).
[44] P. Richet, R.A. Robie, and B.S. Hemingway, Eur. J. Mineral. **3**, 475 (1991).
[45] K. Adamkovičová, L. Kosa, and I. Proks, Silikaty **24**, 193 (1980).
[46] G. Hofmaier, Berg Hutterun Monatsh Montcur Hochsch. Loeben **113**, 1968 (1968).
[47] D.R. Neuville and P. Richet, Geochim. Cosmochim. Acta **55**, 1011 (1991).
[48] T. Licko and V. Danek, Phys. Chem. Glas. **27**, 22 (1986).
[49] J.O. Bockris and D.C. Lowe, Proc. R. Soc. Lond. Math. Phys. Eng. Sci. **226**, 423 (1954).
[50] G. Urbain, Y. Bottinga, and P. Richet, Geochim. Cosmochim. Acta **46**, 1061 (1982).
[51] G.H. Frischat, in *Mass Transp. Phenom. Ceram.*, edited by A.R. Cooper and A.H. Heuer (Springer US, 1975), pp. 285–295.
[52] C.J.R. González Oliver, D.O. Russo, and P.F. James, Phys. Chem.

Glass. **45**, 100 (2004).
[53] C. Kröger and G. Kreitlow, Glas. Ber **29**, 393 (1956).
[54] G.W. Morey and H.E. Merwin, J. Opt. Soc. Am. **22**, 632 (1932).
[55] A.M. Kalinina, V.N. Filipovich, and V.M. Fokin, J. Non-Cryst. Solids **38**, 723 (1980).
[56] A.A. Cabral, A.A.D. Cardoso, and E.D. Zanotto, J. Non-Cryst. Solids **320**, 1 (2003).
[57] O.V. Mazurin, M.V. Streltsina, and T.P. Shvaiko-Shvaikovskaya, *Handbook of Glass Data. Part C. Ternary Silicate Glasses* (Amsterdam: Elsevier, 1987).
[58] L.N. Sheludyakov, Alma-Ata Nauka (1980).
[59] P.B. Moore and S.J. Louisnathan, Z. Für Krist. - Cryst. Mater. **130**, 438 (2015).
[60] A.A. Cabral, C.R. Chinaglia, V.M. Fokin, and E.D. Zanotto, Glass Sci. Technol.-Glastech. Berichte 131 (1998).
[61] A.A. Cabral, V.M. Fokin, E.D. Zanotto, and C.R. Chinaglia, J. Non-Cryst. Solids **330**, 174 (2003).
[62] I. Avramov, R. Keding, and C. Rüssel, J. Non-Cryst. Solids **272**, 147 (2000).
[63] A.A. Cabral, V.M. Fokin, and E.D. Zanotto, J. Non-Cryst. Solids **343**, 85 (2004).
[64] R. Keding and C. Rüssel, J. Non-Cryst. Solids **219**, 136 (1997).
[65] A.A. Cabral Jr., Nucleação, crescimento de cristais e cinética de vitrificação em vidros de silicatos que nucleiam homogeneamente, Ph.D. thesis, Universidade Federal de São Carlos, 2000.
[66] V.P. Klyuev, personal communication (2003) *apud* M.L.F. Nascimento, Problemas correntes sobre nucleação, crescimento de cristais e difusão em vidros, Ph.D. thesis, Universidade Federal de São Carlos, 2004.

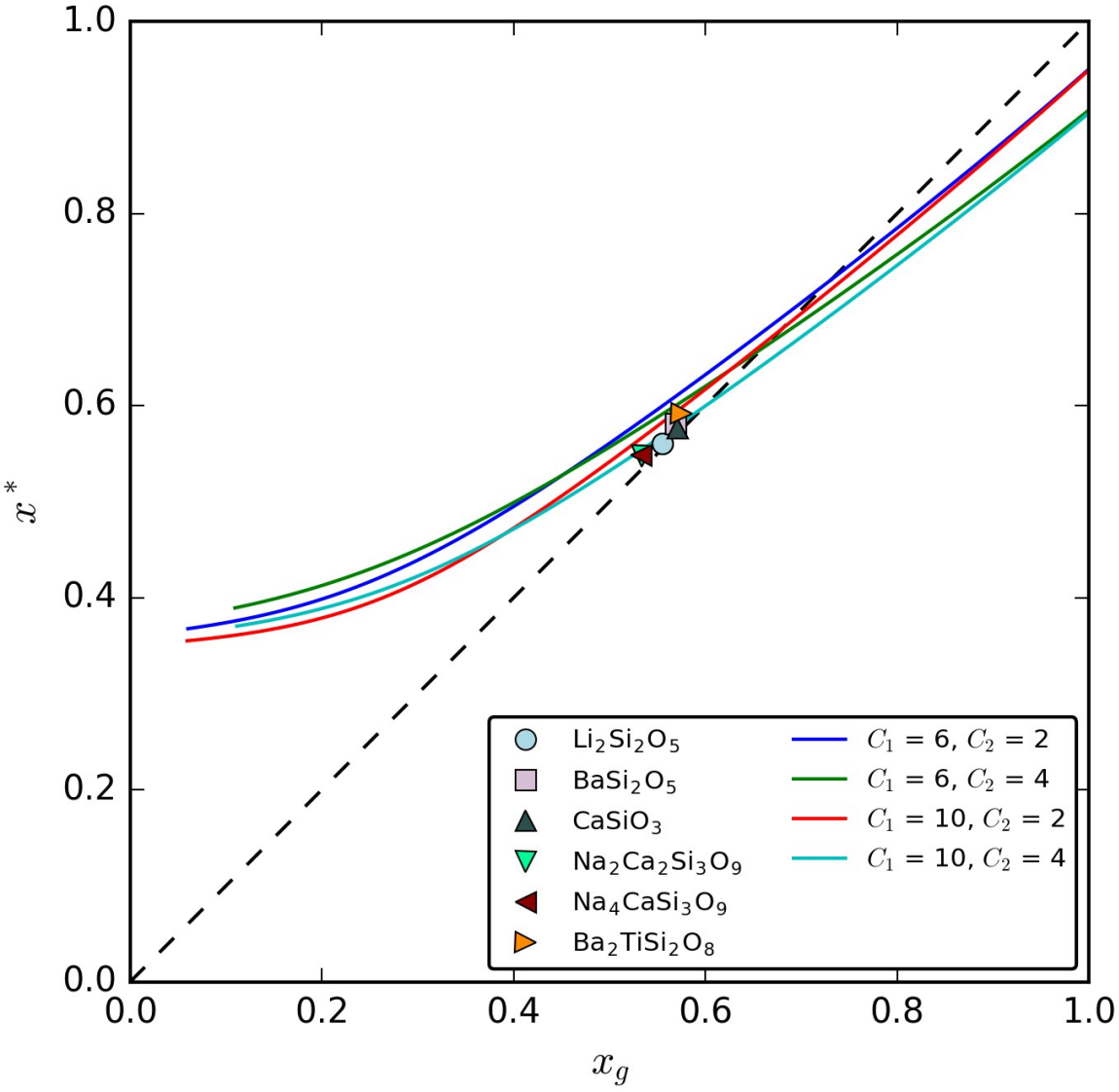

Figure1: Calculated reduced temperature of maximum nucleation rate, x*, versus reduced glass transition temperature, x_g, for typical values of the parameters controlling the thermodynamic barrier (C_1) and the kinetic barrier (C_2) in oxide glass-formers using eqn 19. Experimental data points for six oxide compositions that undergo homogeneous nucleation are shown by symbols. The dotted line refers to $x^* = x_g$. The uncertainty in x_g (see Table I) is smaller than the symbol sizes.

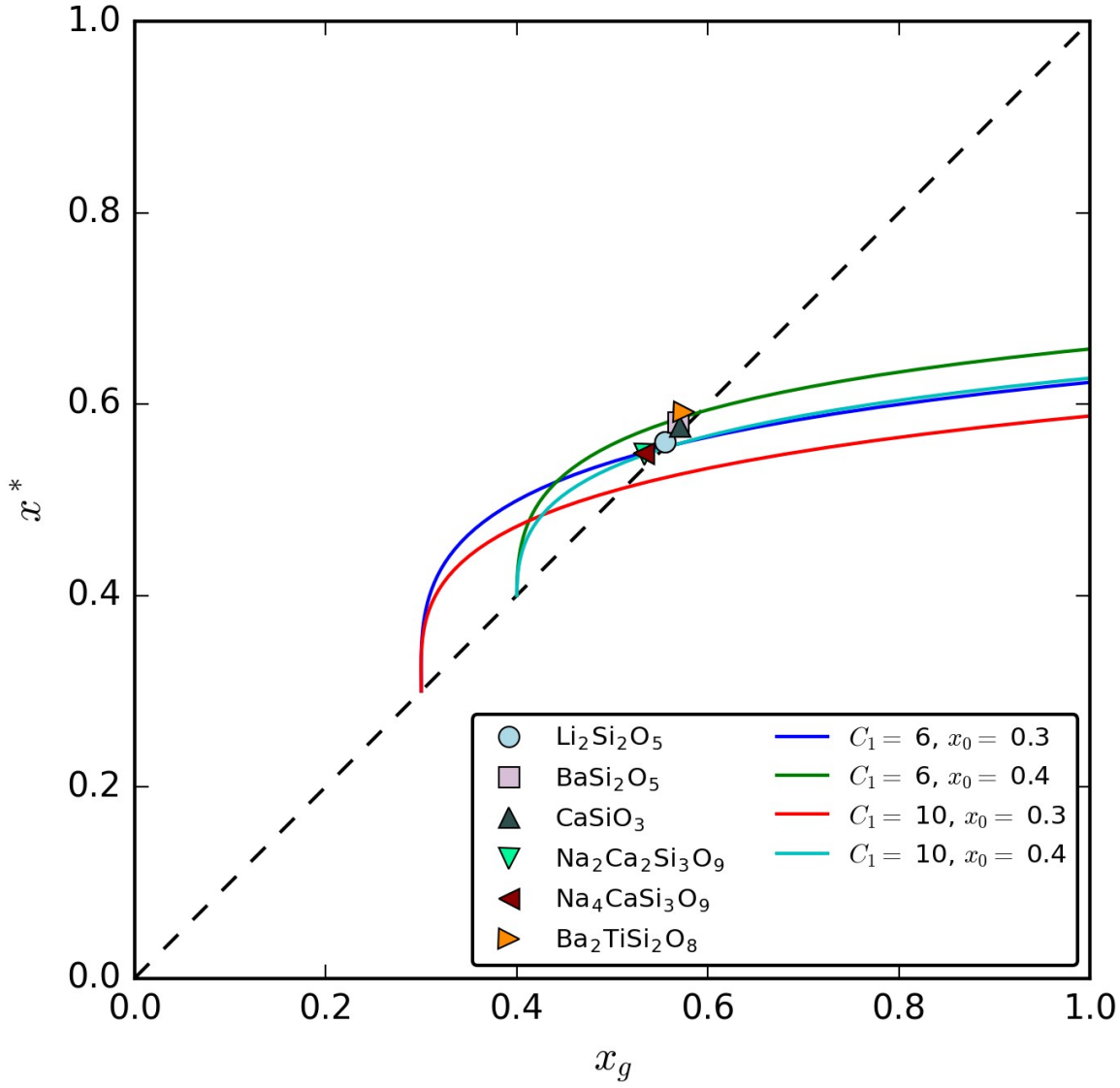

Figure 2: Calculated reduced temperature of maximum nucleation rate, x* versus reduced glass transition temperature, x_g, for different values of the parameters x_o and C_1 using equation 20. Experimental data points for six oxide glasses that undergo internal (homogeneous) nucleation are shown by symbols. The dotted line refers to $x^* = x_g$. The uncertainty in x_g (see Table I) is smaller than the symbol sizes.

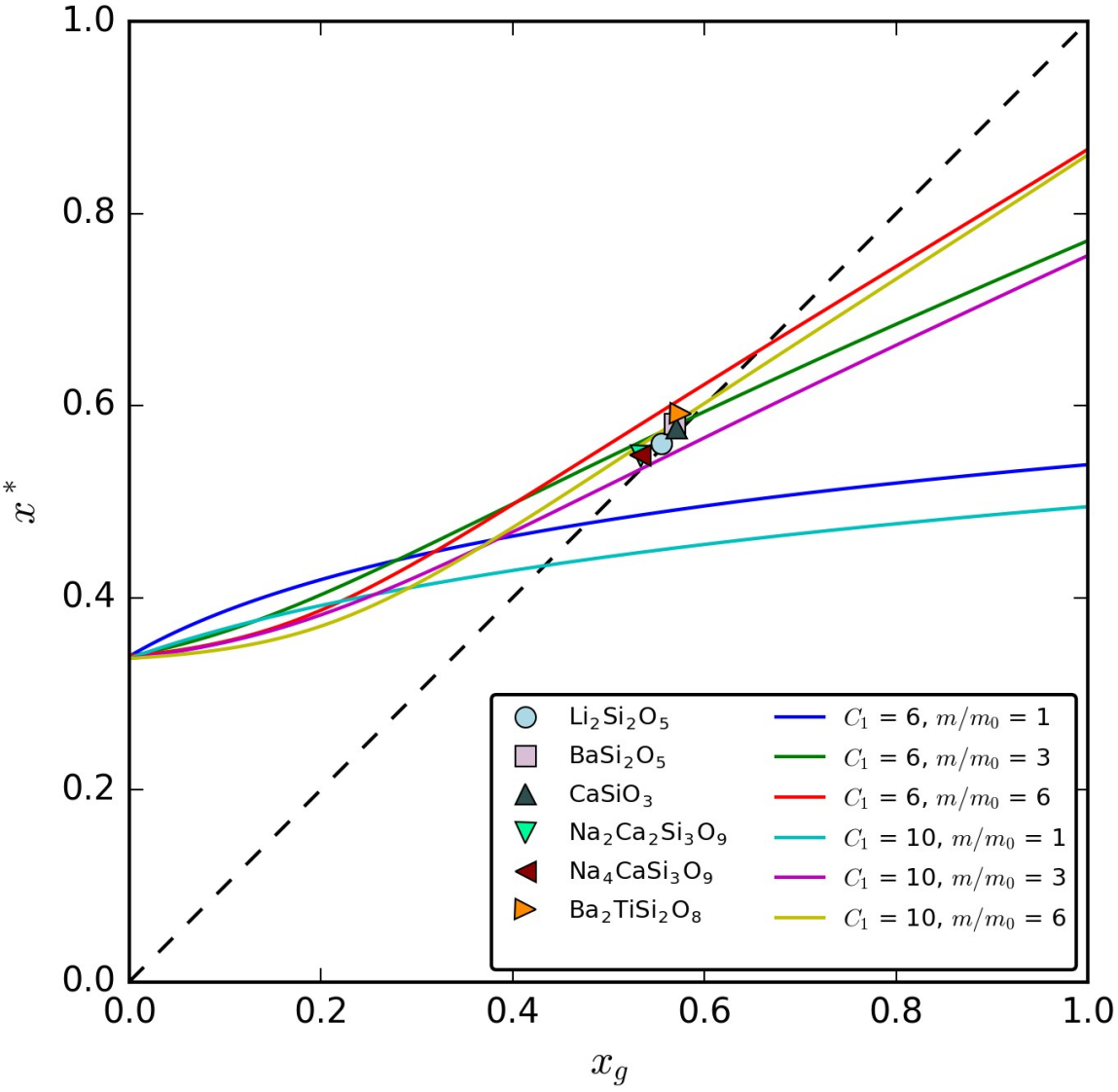

Figure 3: Calculated reduced temperature of maximum nucleation rate, x* versus reduced glass transition temperature, x_g, for different values of the parameters m and C_1 using equation 21. Experimental data points for six oxide glasses that undergo internal (homogeneous) nucleation are shown by symbols. The dotted line refers to $x^* = x_g$ and corresponds to the case when m is infinite. The uncertainty in x_g (see Table I) is smaller than the symbol sizes.

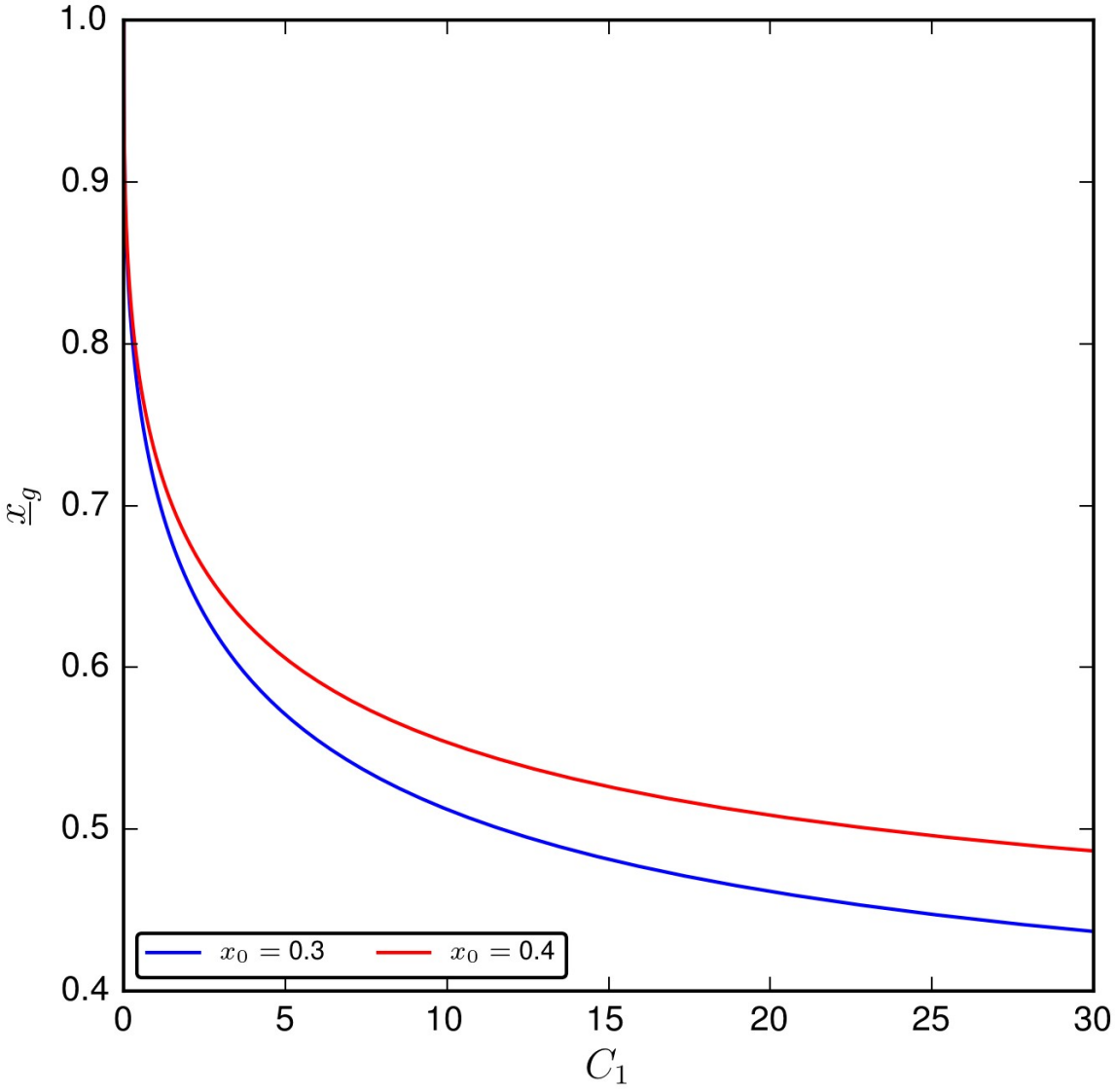

Figure 4: Calculated values of $\underline{x}_g$ as a function of C_1 for two values of x_o using eqn 25. Note that $\underline{x}_g$ increases with increase in x_o and with decrease in C_1.